Satellite-Transition MAS NMR of Low-γ Nuclei at Natural Abundance: Sensitivity, Practical Implementation, and Application to ^{39}K ($I = 3/2$) and ^{25}Mg ($I = 5/2$)

Nicholas G. Dowell,[†] Sharon E. Ashbrook,[‡] and Stephen Wimperis*[,†]

Department of Chemistry, University of Exeter, Stocker Road, Exeter EX4 4QD, United Kingdom, and Department of Earth Sciences, University of Cambridge, Downing Street, Cambridge CB2 3EQ, United Kingdom

Received: May 18, 2004; In Final Form: June 11, 2004

Satellite-transition magic angle spinning (STMAS) is a recently introduced technique for recording high-resolution NMR spectra of quadrupolar nuclei in solids. We present numerical calculations of STMAS signal intensity as a function of radio frequency field strength (ν_1) and spinning rate (ν_R) and show that the sensitivity advantage of STMAS over the older multiple-quantum technique (MQMAS) is greatest for low ν_1 field strengths and high ν_R rates, making STMAS particularly suitable for the study of low-γ nuclei. The practical implementation of STMAS in NMR of low-γ nuclei is discussed and several experimental examples of high-resolution ^{39}K ($I = 3/2$) and ^{25}Mg ($I = 5/2$) NMR spectra are presented, including ^{25}Mg spectra of brucite ($Mg(OH)_2$), diopside ($CaMgSi_2O_6$), and talc ($Mg_3Si_4O_{10}(OH)_2$) recorded at the natural ^{25}Mg abundance of 10%.

Introduction

The multiple-quantum magic angle spinning (MQMAS) NMR technique, introduced by Frydman and Harwood in 1995,[1] has revolutionized the study of many half-integer quadrupolar nuclides in solids. The method allows high-resolution spectra, free from second-order quadrupolar broadening, to be obtained using only conventional MAS probe hardware and has proved itself to be robust, reliable, and relatively easy to implement.[2−4] One area where MQMAS has not been applied with notable success however is in the study of quadrupolar nuclei with low gyromagnetic ratios (γ), usually (but arbitrarily) defined[5] to be those nuclei that have a Larmor frequency ($\nu_0 = \gamma B_0/2\pi$) less than 40 MHz at a static magnetic field strength of $B_0 = 9.4$ T. Examples of physical, chemical, mineralogical, and materials interest include ^{35}Cl, ^{39}K ($I = 3/2$), ^{25}Mg, ^{47}Ti, and ^{95}Mo ($I = 5/2$).

It is easy to list the reasons why MQMAS has had very limited application to low-γ quadrupolar nuclei. The sensitivity of the basic NMR experiment is generally considered to be proportional to γ^3, making low-γ nuclei difficult to observe even using conventional techniques. The sensitivity of the MQMAS method is known to be poor unless high radio frequency field strengths ($\nu_1 = \gamma B_1/2\pi$) are available, especially for the multiple- to single-quantum "reconversion" pulse,[6] yet such high ν_1 field strengths are clearly difficult to achieve when γ is small. And, finally, multiple-quantum coherences can be excited with greatest efficiency when MAS rates (ν_R) are low,[7] but low-γ nuclei will tend to exhibit large second-order quadrupolar broadenings (proportional to $1/\nu_0$) and high MAS rates are desirable.

In 2000, Gan introduced an alternative MAS-based method of recording high-resolution NMR spectra of half-integer quadrupolar nuclei in solids.[8] One reason this satellite-transition magic angle spinning (STMAS) technique is of great interest is that it has been shown experimentally to yield a significant sensitivity advantage over the MQMAS experiment when applied to such "routine" quadrupolar nuclei as ^{23}Na, ^{87}Rb ($I = 3/2$), ^{17}O, and ^{27}Al ($I = 5/2$).[9−12] In view of the difficulty of applying MQMAS to low-γ nuclei, the question naturally arises as to whether this STMAS sensitivity advantage persists with low-γ nuclei (i.e., at low ν_1 field strengths and high ν_R rates) and, if so, whether it is larger or smaller than it is for the more routine nuclei.

The purpose of this paper is to investigate the suitability of STMAS as a method for obtaining high-resolution NMR spectra of low-γ quadrupolar nuclei. First, the relative sensitivity of STMAS and MQMAS is studied as a function of radio frequency field strength (ν_1) and MAS rate (ν_R) using numerical calculations. Next, the practical implementation of the STMAS technique on low-γ nuclei is discussed. Finally, examples are presented of ^{39}K ($I = 3/2$, $\nu_0 = 18.7$ MHz at $B_0 = 9.4$ T) and ^{25}Mg ($I = 5/2$, $\nu_0 = 24.5$ MHz at $B_0 = 9.4$ T) STMAS NMR spectra, with both nuclides present at natural abundance (93% for ^{39}K and 10% for ^{25}Mg).

Numerical Calculations

The two high-resolution methods we will compare are the STMAS experiment in Figure 1a[9] and the triple-quantum MAS experiment in Figure 1b.[4] These phase-modulated split-t_1 methods are probably the most sensitive basic implementations of the two-dimensional STMAS and MQMAS techniques.[4,9] An initial radio frequency pulse (p1) excites either inner satellite-transition (ST) coherence ($m_I = \pm 1/2 \leftrightarrow \pm 3/2$, with coherence order $p = +1$) or triple-quantum (TQ) coherence ($m_I = -3/2 \leftrightarrow +3/2$, with $p = +3$) from a thermal equilibrium state (I_z). These coherences then evolve during an evolution period before being converted into central-transition (CT) coherence ($m_I = -1/2 \leftrightarrow +1/2$, with $p = +1$) by a second radio frequency pulse

* To whom correspondence should be addressed. Fax: +44-1392-263434. E-mail: s.wimperis@exeter.ac.uk.
[†] University of Exeter.
[‡] University of Cambridge.

10.1021/jp047868m CCC: $27.50
Published on Web 08/10/2004

(p2). After a further free-precession period, a third radio frequency pulse (p3), which has a relatively low radio frequency field strength ($\nu_1 \sim 10$ kHz),[2] changes the sign of the CT coherence order from $p = +1$ to $p = -1$ and allows the signal to be detected in the t_2 acquisition period as a spin echo.[2,4]

Since the two experiments in Figure 1 are identical after the second pulse, any sensitivity difference between them arises as a result of the different coherence transfer efficiencies during the first and second pulses. We can calculate the effect of these pulses using the solution to the Liouville−von Neumann equation:

$$\sigma^+ = U(\tau_p)\sigma^- U(\tau_p)^{-1} \tag{1a}$$

$$U(\tau_p) = T\exp\{-i\int_0^{\tau_p} H(t)\,dt\} \tag{1b}$$

where σ^- and σ^+ are the spin density operators before and after the pulse, respectively; T is the Dyson time-ordering operator; τ_p is the duration of the pulse; and $H(t)$ is the rotating-frame Hamiltonian during the pulse. For the first pulse, $\sigma^- = I_z$ for both experiments, while for the second pulse $\sigma^- = |+1/2\rangle\langle+3/2|$ for STMAS and $\sigma^- = |-3/2\rangle\langle+3/2|$ for MQMAS. The relevant component of σ^+ is extracted by calculating the expectation value:

$$\langle A\rangle = Tr\{\sigma^+ A^+\} \tag{2}$$

where A is the (non-hermitian) observable operator and A^+ is its adjoint, and where for the first pulse $A_{I_z\rightarrow ST} = |+1/2\rangle\langle+3/2|$ for STMAS and $A_{I_z\rightarrow TQ} = |-3/2\rangle\langle+3/2|$ for MQMAS, while for the second pulse $A_{ST\rightarrow CT} = A_{TQ\rightarrow CT} = |-1/2\rangle\langle+1/2|$.

The rotating-frame Hamiltonian during the pulse that we will use is

$$H(t) = 2\pi\nu_1 I_x + 2\pi\nu_Q(t)\{I_z^2 - I(I+1)/3\} \tag{3}$$

For the special case of MAS, the first-order quadrupolar splitting parameter $\nu_Q(t)$ can be written:

$$\nu_Q(t) = \frac{\nu_Q^{PAS}}{2}\{-\sqrt{2}\sin 2\theta\cos(2\pi\nu_R t + \xi) + \sin^2\theta\cos 2(2\pi\nu_R t + \xi)\} \tag{4a}$$

$$\nu_Q^{PAS} = \frac{3e^2qQ}{4I(2I-1)h} \tag{4b}$$

where θ is the orientation of the quadrupole tensor with respect to the rotor axis and ξ is its phase about that axis when $t = 0$. For simplicity, an axially symmetric quadrupolar tensor ($\eta = 0$) has been assumed in eq 4.

The presence of the large first-order quadrupolar splitting in the satellite transitions produces a very strong phase variation in the (complex) expectation values $\langle A_{I_z\rightarrow ST}\rangle$ and $\langle A_{ST\rightarrow CT}\rangle$ as a function of θ, ξ. In a real experiment, this phase variation is fully refocused (for short pulse durations) by the combination of MAS and precise rotor synchronization, but in numerical calculations of the type used here it will produce misleading results unless the powder averaging over θ, ξ is performed with care. Our approach to this is to assume full refocusing of the phase variation (in the short-pulse limit) by taking the modulus of the expectation value (i.e., mod$\{\langle A\rangle\}$) before powder averaging. Thus, we can represent the coherence transfer efficiency of a single pulse by

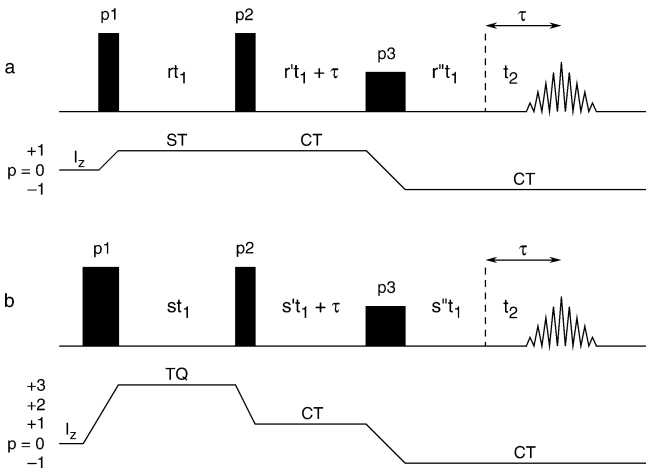

Figure 1. Pulse sequences and coherence pathway diagrams for the phase-modulated split-t_1 (a) STMAS and (b) triple-quantum MAS NMR experiments compared and implemented in this work. For spin $I = 3/2$: $r = 9/17$, $r' = 8/17$, $r'' = 0$ and $s = 9/16$, $s' = 7/16$, $s'' = 0$. For spin $I = 5/2$: $r = 24/31$, $r' = 0$, $r'' = 7/31$ and $s = 12/31$, $s' = 0$, $s'' = 19/31$.

$$S_{X\rightarrow Y}(\tau_p) = \int_{\theta=0}^{180^\circ}\int_{\xi=0}^{360^\circ} \mathrm{mod}\{\langle A_{X\rightarrow Y}\rangle(\theta,\xi,\tau_p)\}\sin\theta\,d\theta\,d\xi \tag{5}$$

and over the first and second pulses in either an STMAS or MQMAS experiment by

$$S_{I_z\rightarrow Y\rightarrow CT}(\tau_{p1},\tau_{p2}) = \int_{\theta=0}^{180^\circ}\int_{\xi=0}^{360^\circ} \mathrm{mod}\{\langle A_{I_z\rightarrow Y}\rangle(\theta,\xi,\tau_{p1})\}\,\mathrm{mod}\{\langle A_{Y\rightarrow CT}\rangle(\theta,\xi,\tau_{p2})\}\sin\theta\,d\theta\,d\xi \tag{6}$$

The two pulse durations in eq 6 should be optimized globally but, as in an actual experiment, we can approximately achieve this by first optimizing the excitation pulse in eq 5 to obtain τ_{p1}^{opt} and then the reconversion pulse in eq 6 to obtain τ_{p2}^{opt}. The relative sensitivity of STMAS and MQMAS can now be expressed as the ratio

$$R^{ST/TQ} = \frac{2S_{I_z\rightarrow ST\rightarrow CT}(\tau_{p1}^{opt},\tau_{p2}^{opt})}{S_{I_z\rightarrow TQ\rightarrow CT}(\tau_{p1}^{opt},\tau_{p2}^{opt})} \tag{7}$$

where the factor of 2 allows for the existence of two satellite transitions, $m_I = +1/2 \leftrightarrow +3/2$ and $m_I = -1/2 \leftrightarrow -3/2$, in an STMAS experiment but just the one TQ transition, $m_I = -3/2 \leftrightarrow +3/2$, in an MQMAS experiment. Note that eq 7 is not intended to imply that the optimum pulse durations (τ_p^{opt}) are the same in an STMAS experiment as they are in an MQMAS experiment.

Figure 2a shows plots of $R^{ST/TQ}$ for spins $I = 3/2$ and 5/2 as a function of the ratio of the radio frequency field strength to the quadrupolar parameter (i.e., ν_1/ν_Q^{PAS}), while Figure 2b shows the individual curves $2S_{I_z\rightarrow ST\rightarrow CT}(\tau_{p1}^{opt},\tau_{p2}^{opt})$ and $S_{I_z\rightarrow TQ\rightarrow CT}(\tau_{p1}^{opt},\tau_{p2}^{opt})$ for comparison. For these calculations, the MAS rate was assumed to be so low that the rotor was effectively static during the pulses (i.e., $2\pi\nu_R \ll \tau_p^{-1}$). The following points may be noted: (i) the sensitivity ratio $R^{ST/TQ}$ is always greater than 2 and rises above 3 when $\nu_1/\nu_Q^{PAS} \lesssim 0.15$ (further calculations show that this is mainly because the

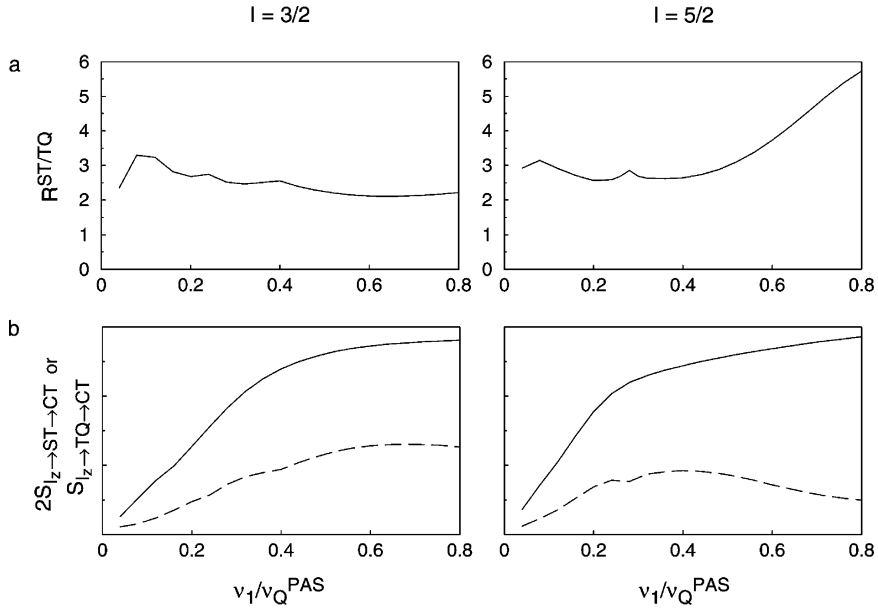

Figure 2. Numerical calculations of (a) $R^{ST/TQ}$, the ratio of the STMAS sensitivity parameter ($2S_{I_z\rightarrow ST\rightarrow CT}$) to the MQMAS sensitivity parameter ($S_{I_z\rightarrow TQ\rightarrow CT}$), and (b) the individual parameters $2S_{I_z\rightarrow ST\rightarrow CT}$ (solid line) and $S_{I_z\rightarrow TQ\rightarrow CT}$ (dashed line) for spins $I = 3/2$ and 5/2 plotted as a function of ν_1/ν_Q^{PAS}). Calculations assume limit of very slow MAS ($\nu_R \sim 0$) and pulse durations optimized for each individual ν_1 value. Home-written software was used.

STMAS reconversion pulse is more effective at low ν_1 field strengths than the MQMAS reconversion pulse); (ii) despite the increase in $R^{ST/TQ}$, Figure 2b acts as a reminder that the absolute sensitivities of both STMAS and MQMAS decrease rapidly as the ratio ν_1/ν_Q^{PAS} decreases; and (iii) the large magnitudes of $R^{ST/TQ}$ found at high ν_1/ν_Q^{PAS} values for spin $I = 5/2$ (originating mainly from the decrease in $S_{I_z\rightarrow TQ\rightarrow CT}(\tau_{p1}^{opt}, \tau_{p2}^{opt})$ for $\nu_1/\nu_Q^{PAS} > 0.4$) are misleading in that they represent the well-known failure of a single pulse to excite TQ coherence when the ν_1 field is too strong[13] (similar behavior is found for spin $I = 3/2$ when $\nu_1/\nu_Q^{PAS} > 0.8$); a good experimentalist would keep this high ν_1 field strength for the reconversion pulse but turn the power down for the excitation pulse.

The STMAS sensitivity advantage of a factor of between 2 and 3.5 found in Figure 2 is somewhat lower than that found experimentally for nuclei such as ^{87}Rb ($I = 3/2$), ^{17}O, ^{27}Al ($I = 5/2$), and ^{93}Nb ($I = 9/2$) under conditions of fast MAS (i.e., $\nu_R \geq 20$ kHz), where factors of between 4 and 6 are commonly found.[9,12] The cause of this apparent discrepancy is the assumption of very slow MAS, $\nu_R \sim 0$, in Figure 2. This assumption can be relaxed by using a realistic MAS rate in the quadrupolar splitting parameter in eq 4 and performing the integration in eq 1 in a piecewise fashion over the pulse duration τ_p. Figure 3 shows plots of the excitation pulse efficiencies $S_{I_z\rightarrow ST}(\beta_1 = 2\pi\nu_1\tau_{p1})$ and $S_{I_z\rightarrow TQ}(\beta_1 = 2\pi\nu_1\tau_{p1})$ and of the reconversion pulse efficiencies $S_{ST\rightarrow CT}(\beta_2 = 2\pi\nu_1\tau_{p2})$ and $S_{TQ\rightarrow CT}(\beta_2 = 2\pi\nu_1\tau_{p2})$ for spins $I = 3/2$ and 5/2 as a function of the inherent pulse flip $\beta = 2\pi\nu_1\tau_p$ for MAS rates between 0 (static) and 40 kHz. The following points may be noted: (i) the excitation efficiency of ST coherence (Figure 3a) is virtually independent of MAS rate, while that of TQ coherence (Figure 3b) decreases rapidly as the MAS rate increases,[7] most notably for spin $I = 3/2$; and (ii) the STMAS and MQMAS reconversion efficiencies in Figure 3, panels c and d, are almost independent of the MAS rate.

Practical Implementation

^{39}K ($I = 3/2$) and ^{25}Mg ($I = 5/2$) STMAS NMR were implemented on a Bruker Avance 400 spectrometer equipped with 1 kW radio frequency amplifiers and a widebore 9.4 T magnet. The phase-modulated split-t_1 STMAS experiment shown in Figure 1a was used,[9,12] as described in the previous section: this has the additional advantage that the signal is detected in t_2 as an echo and problems with acoustic ringing[14] can be avoided. Two probes were used: either a Bruker 7-mm MAS probe specially optimized for low-γ nuclei (X-channel tunable from 18 to 95 MHz) or a Bruker 4-mm MAS probe "borrowed" from a 4.7 T magnet (X-channel tunable from 18 to 82 MHz). We used MAS rates of either 7 kHz (7-mm rotor) or 12.5 kHz (4-mm rotor), close to the maximum achievable on these probes. Higher MAS rates would be desirable, however, owing to the large second-order quadrupolar broadenings found for low-γ nuclei.

The STMAS technique requires that the spinning angle on the probe is set to the magic angle (54.736°) with a very high degree of precision (±0.002°).[8,9,12] Normally, we use a ^{87}Rb ($I = 3/2$, $\nu_0 = 130.9$ MHz at $B_0 = 9.4$ T, 28% natural abundance) STMAS NMR experiment, performed on $RbNO_3$, to set the spinning angle and then use the pneumatic insert/eject system to change to a rotor filled with the material of interest.[9] Here, however, as neither probe could tune to the ^{87}Rb frequency, the easily observable ^{85}Rb ($I = 5/2$, $\nu_0 = 38.6$ MHz at $B_0 = 9.4$ T, 72% natural abundance) STMAS signal from $RbNO_3$ was used instead. The impact caused by dropping a 7-mm (and sometimes even a 4-mm) rotor down the insert tube tends to knock the spinning angle away from the magic angle and so a flow of bearing or eject gas was used to cushion the fall of the rotor during insertion.[12]

For the highest sensitivity, the pulse durations in an STMAS experiment should be optimized and normally, for a routine quadrupolar nucleus, this is done on the material of interest or on one containing nuclei with similar NMR parameters. For ^{39}K and ^{25}Mg STMAS NMR, we were able to calibrate the third (low-power) pulse by simple (selective) nutation, using either K_2SO_4 or $Mg(OH)_2$ enriched to 98 at. % in ^{25}Mg. However, there was insufficient sensitivity to optimize the first and second STMAS pulses in the conventional manner[9,12] on these solids. Instead, we calibrated the ν_1 field strength by simple (nonselective) nutation, using either KBr or MgO, where ^{39}K and ^{25}Mg

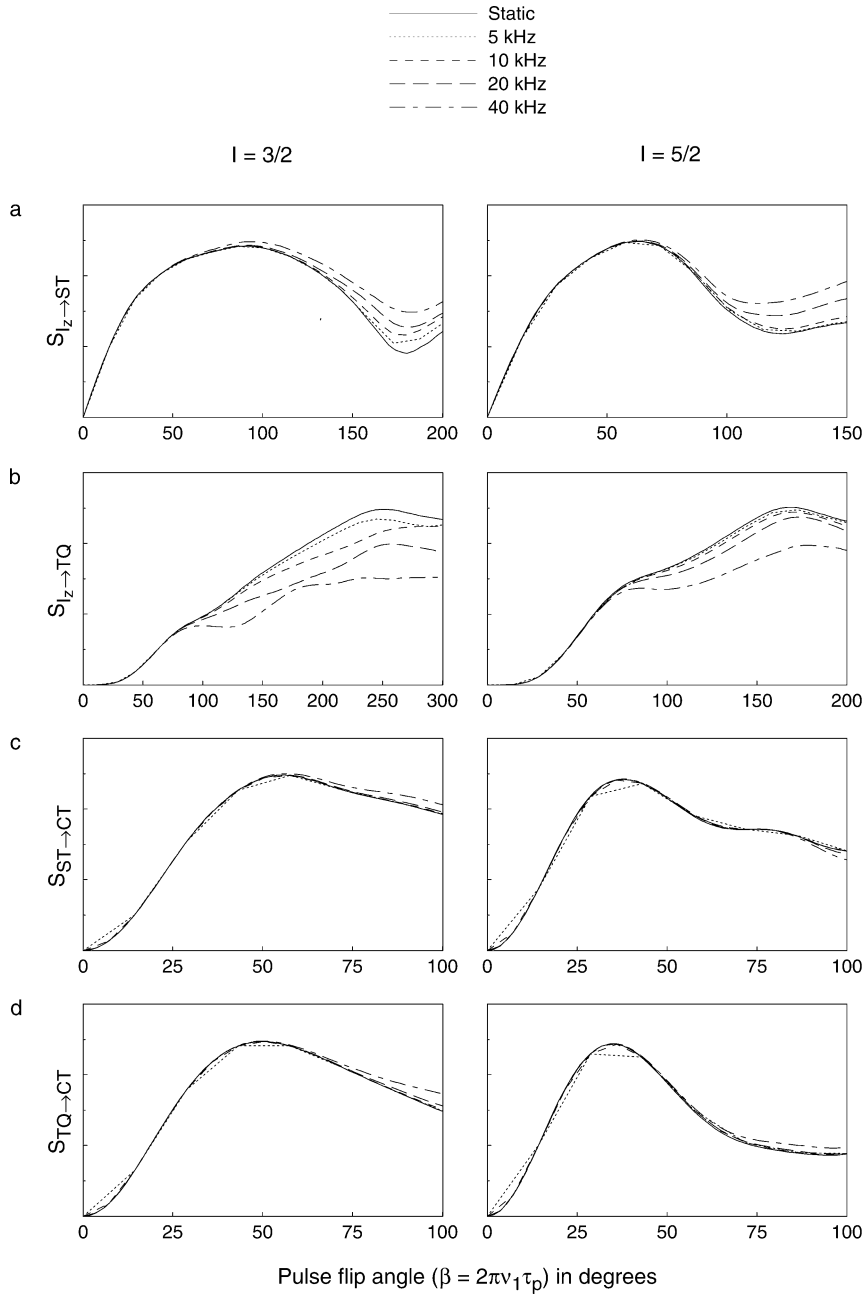

Figure 3. Numerical calculations of (a) $S_{I_z\rightarrow ST}$, the excitation efficiency of the first STMAS pulse; (b) $S_{I_z\rightarrow TQ}$, the excitation efficiency of the first MQMAS pulse; (c) $S_{ST\rightarrow CT}$, the reconversion efficiency of the second STMAS pulse; and (d) $S_{TQ\rightarrow CT}$, the reconversion efficiency of the second MQMAS pulse plotted as a function of the inherent pulse flip angle $\beta = 2\pi\nu_1\tau_p$ for spin $I = 3/2$ and 5/2 and for a range of MAS rates between 0 (static) and 40 kHz. The $\nu_1 = \gamma B_1/2\pi$ radio frequency field strength was 100 kHz, and ν_Q^{PAS} was 500 kHz. Home-written software was used.

are in symmetric environments and exhibit no significant quadrupolar splittings. These solids provide good sensitivity under MAS, even at natural abundance, despite their long T_1 time constants. The maximum field strengths were estimated as $\nu_1 = 25$ kHz on the 7-mm and 40 kHz on the 4-mm probe for ^{39}K and $\nu_1 = 31$ kHz on the 7-mm and 50 kHz on the 4-mm probe for ^{25}Mg. We could then set the first and second STMAS pulse durations using the results of the numerical calculations described above, which indicate that $\beta_1^{opt} = 2\pi\nu_1\tau_{p1}^{opt} \approx 90°$ and $\beta_2^{opt} \approx 60°$ for spin $I = 3/2$ and $\beta_1^{opt} \approx 70°$and $\beta_2^{opt} \approx 40°$for spin $I = 5/2$.

High-Resolution ^{39}K and ^{25}Mg NMR Results

Despite its lower Larmor frequency ($\nu_0 = 18.7$ MHz at $B_0 = 9.4$ T), ^{39}K is a much easier nucleus than ^{25}Mg to observe in unenriched materials owing to its high natural abundance (93%). Figure 4a shows the ^{39}K MAS NMR spectrum of arcanite (K_2SO_4) recorded with a spin-echo pulse sequence. The spectrum appears to consist of at least two unresolved second-order quadrupolar line shapes, consistent with the two inequivalent K sites predicted from the XRD structure.[15] The high-resolution ^{39}K STMAS NMR spectrum, shown in Figure 4b together with its isotropic projection, was recorded in 38 h and reveals two inequivalent K sites with the expected 1:1 intensities in the projection. Figure 4c shows the individual δ_2 line shapes extracted from the two-dimensional STMAS spectrum in Figure 4b and fitted with model second-order quadrupolar line shapes. These fittings, together with analysis of the δ_1 and δ_2 shifts of the centers-of-mass of the ridge line shapes,[2,12] yield isotropic chemical shifts, quadrupolar coupling constants, and asymmetry

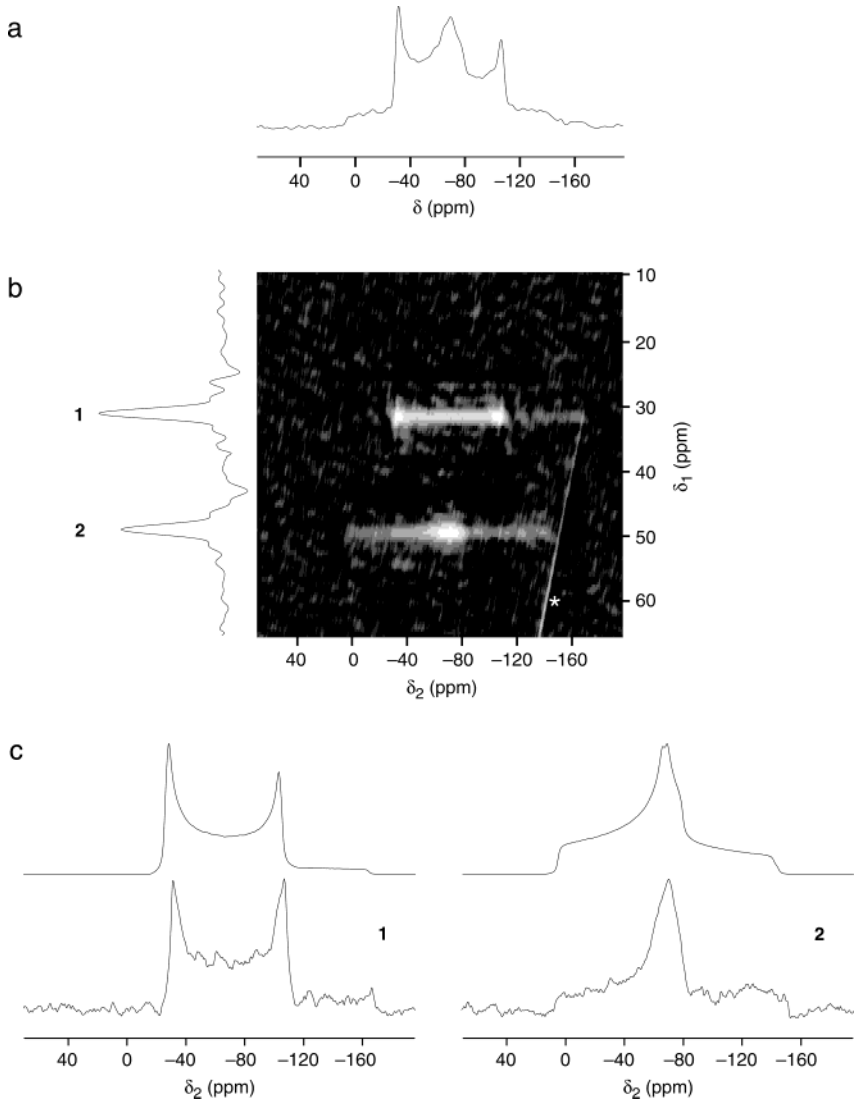

Figure 4. ^{39}K ($\nu_0 = 18.7$ MHz) MAS NMR of arcanite (K_2SO_4). (a) Spin-echo spectrum recorded with $\nu_R = 7$ kHz on a 7-mm MAS probe (2048 transients summed with relaxation interval of 2 s). (b) Split-t_1 STMAS spectrum, together with its isotropic projection, recorded with $\nu_R = 7$ kHz on a 7-mm MAS probe (704 transients summed for each of 96 t_1 increments of 269.8 μs; relaxation interval of 2 s). (c) δ_2 line shapes extracted from the STMAS spectrum and fitted with model second-order quadrupolar line shapes. The (aliased) autocorrelation STMAS diagonal in panel b is marked with an asterisk. Chemical shifts referenced to aqueous KCl (via KBr MAS peak at 55 ppm).[5]

parameters of $\delta_{CS} = -6$ ppm, $C_Q = e^2qQ/h = 0.95$ MHz, $\eta = 0.05$ for site 1 and $\delta_{CS} = 6$ ppm, $C_Q = 0.85$ MHz, $\eta = 0.95$ for site 2 in Figure 4, in agreement with ref 16. Despite several attempts, we were unable to obtain a meaningful ^{39}K MQMAS NMR spectrum from arcanite at $B_0 = 9.4$ T.

It is chiefly the low natural abundance (10%) that makes ^{25}Mg ($\nu_0 = 24.5$ MHz at $B_0 = 9.4$ T) a particularly daunting prospect for high-resolution NMR spectroscopy in solids. Therefore, the ^{25}Mg STMAS and MQMAS experiments were compared on brucite ($Mg(OH)_2$) enriched to 98 at. % in ^{25}Mg. Figure 5a shows the ^{25}Mg spin-echo MAS NMR spectrum of enriched brucite, which consists of the expected (from the XRD structure[17]) single second-order quadrupolar line shape. The fitting of this line shape yields $\delta_{CS} = 10$ ppm, $C_Q = 3.1$ MHz, and $\eta = 0.05$, in agreement with refs 18 and 19. The ^{25}Mg MQMAS and STMAS NMR spectra of enriched brucite, shown in Figure 5b together with their isotropic projections and extracted δ_2 line shapes, were recorded in 19 and 6 h, respectively, with identical resolution in t_1 and t_2. The STMAS spectrum has roughly a factor of 2 better signal-to-noise ratio despite being (i) recorded in less than one-third of the total acquisition time for the MQMAS spectrum and (ii) broadened in the δ_1 dimension by a third-order quadrupolar interaction[12,20] (the presence of this interaction, which affects only satellite transitions, in $Mg(OH)_2$ has been confirmed by computer simulation[21]). By comparison with Figure 5a, it can also be seen that the δ_2 line shape extracted from the STMAS spectrum is less distorted than that from the MQMAS spectrum.

Having confirmed the successful implementation of the ^{25}Mg STMAS experiment and its sensitivity advantage over MQMAS, we investigated the feasibility of high-resolution ^{25}Mg NMR at natural abundance on a number of nonenriched materials, with brucite being the obvious first choice. Figure 5c shows the ^{25}Mg spin-echo MAS spectrum (recorded in 17 min) and the ^{25}Mg STMAS NMR spectrum of nonenriched brucite (recorded in 66 h) together with its isotropic projection. The latter reproduces exactly the STMAS spectrum of the enriched material in Figure 5b, including the details of the third-order splitting in the δ_1 dimension, demonstrating that high-resolution ^{25}Mg NMR spectra are obtainable at natural abundance using the STMAS technique, even at static magnetic field strengths as modest as $B_0 = 9.4$ T.

Figure 6a shows the ^{25}Mg spin-echo MAS NMR spectrum of nonenriched diopside ($CaMgSi_2O_6$) recorded in 20 h. Fitting

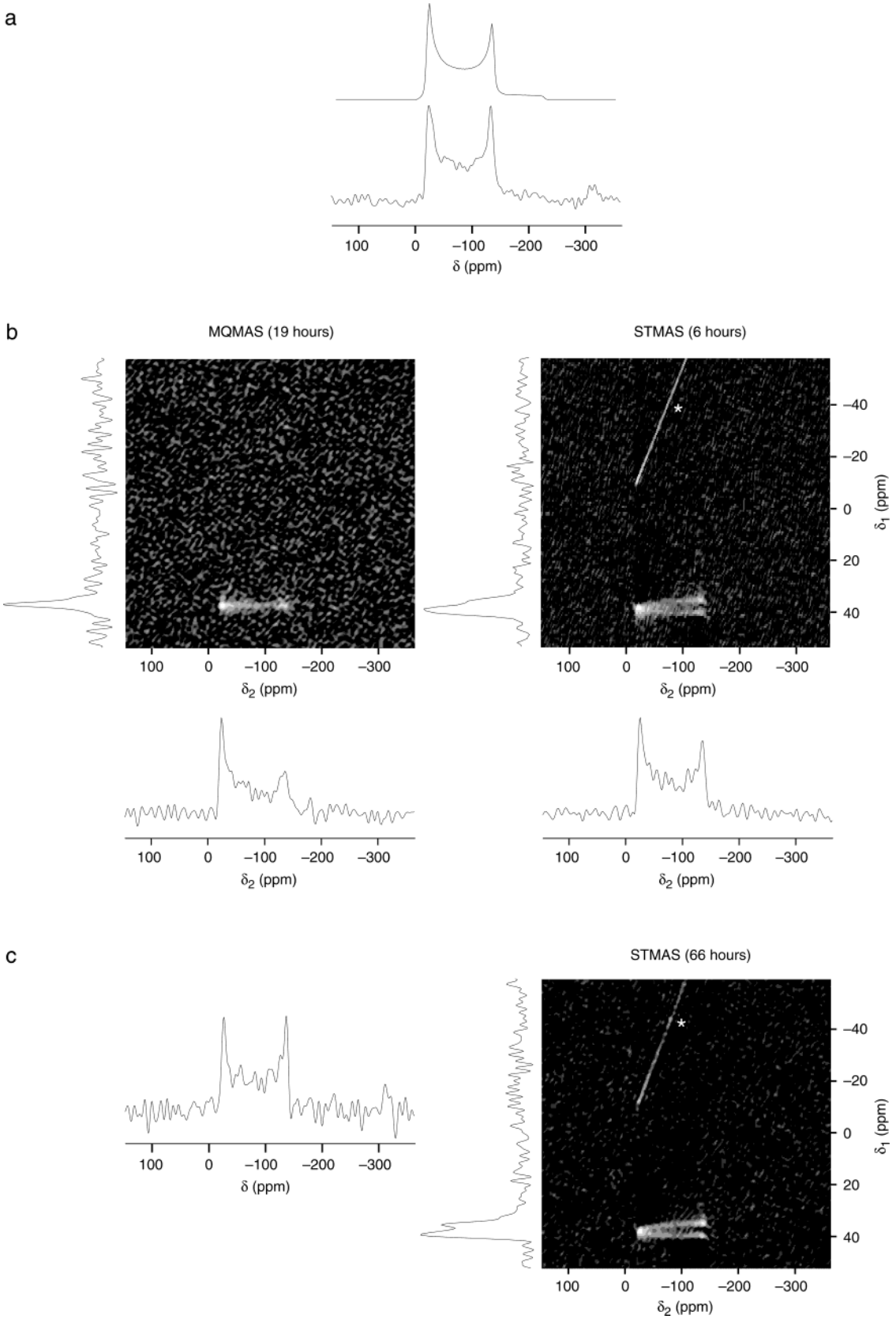

Figure 5. ^{25}Mg ($\nu_0 = 24.5$ MHz) MAS NMR of brucite ($Mg(OH)_2$). (a) Spin-echo spectrum (with fitting) of 98 at. % ^{25}Mg-enriched material (∼100 mg) recorded with $\nu_R = 7$ kHz on a 7-mm MAS probe (1024 transients summed with relaxation interval of 1 s; ^1H decoupled). (b) Split-t_1 MQMAS and STMAS spectra of enriched material (∼100 mg), together with their isotropic projections and extracted δ_2 line shapes recorded with $\nu_R = 12.5$ kHz on a 4-mm MAS probe (MQMAS: 672 transients summed for each of 86 t_1 increments of 206.7 μs; relaxation interval of 1.2 s. STMAS: 96 transients summed for each of 172 t_1 increments of 103.3 μs; relaxation interval of 1.2 s). (c) Spin-echo spectrum (1024 transients summed with relaxation interval of 1 s; ^1H decoupled) and split-t_1 STMAS spectrum (2048 transients summed for each of 96 t_1 increments of 184.5 μs; relaxation interval of 1.2 s; ^1H decoupled), together with its isotropic projection, of nonenriched brucite (∼400 mg) recorded with $\nu_R = 7$ kHz on a 7-mm MAS probe. The autocorrelation STMAS diagonals in panels b and c are marked with asterisks. Chemical shifts referenced to aqueous $MgSO_4$ (via MgO MAS peak at 26 ppm).[5]

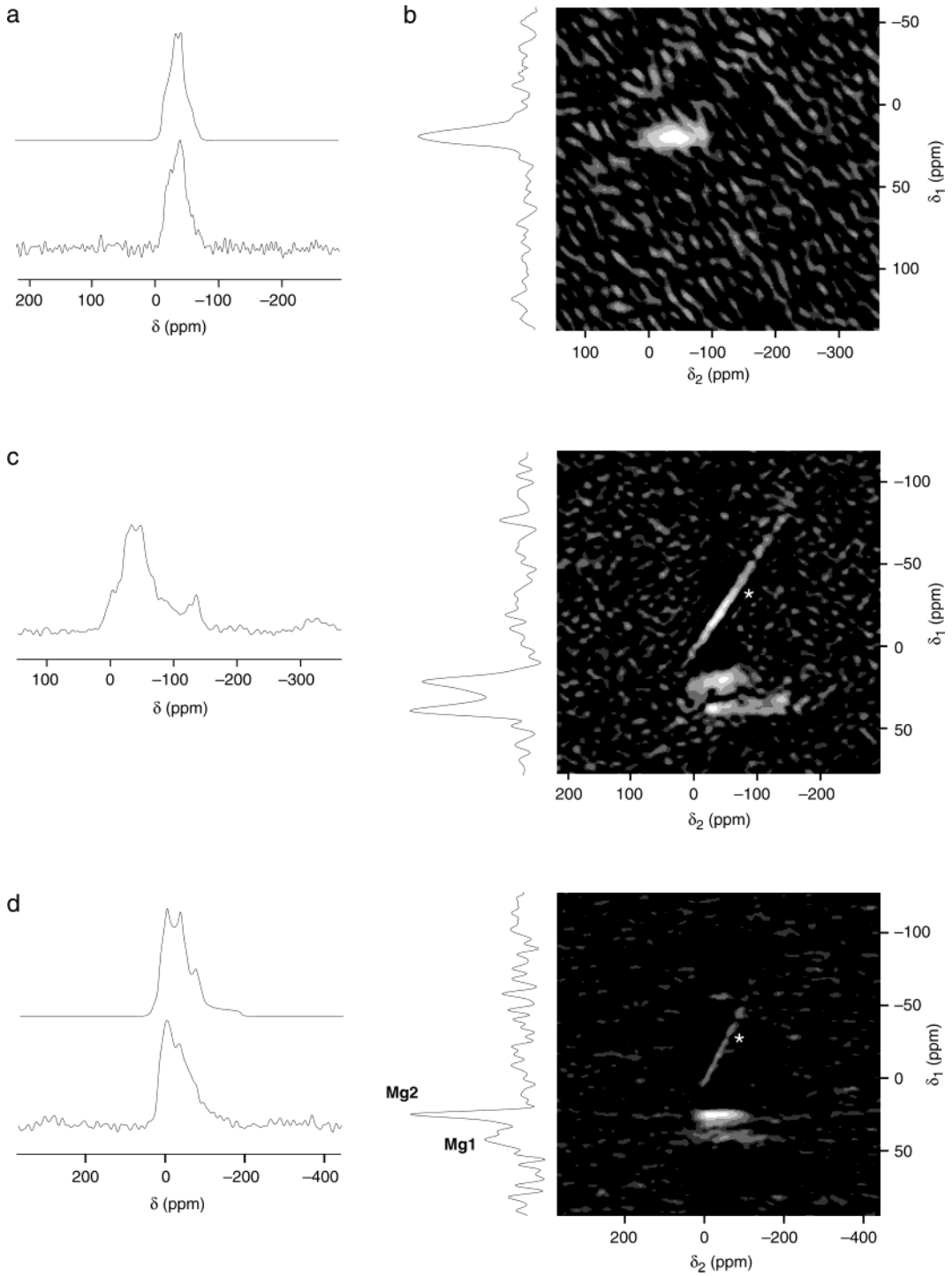

Figure 6. Natural abundance ^{25}Mg ($\nu_0 = 24.5$ MHz) MAS NMR spectra of (a, b) diopside ($CaMgSi_2O_6$), (c) a 1:1 Mg at. % mixture of brucite and diopside, and (d) talc ($Mg_3Si_4O_{10}(OH)_2$). (a) Spin-echo spectrum (with fitting) recorded with $\nu_R = 12.5$ kHz on a 4-mm MAS probe (73728 transients summed with relaxation interval of 1 s). (b) Split-t_1 STMAS spectrum, together with its isotropic projection, recorded with $\nu_R = 12.5$ kHz on a 4-mm MAS probe (2400 transients summed for each of 48 t_1 increments of 103.3 μs; relaxation interval of 1 s). (c) Spin-echo spectrum ($\nu_R = 7$ kHz on a 7-mm MAS probe: 73728 transients summed with relaxation interval of 1 s; ^{1}H decoupled) and split-t_1 STMAS spectrum ($\nu_R = 12.5$ kHz on a 4-mm MAS probe: 6016 transients summed for each of 48 t_1 increments of 103.3 μs; relaxation interval of 1 s), together with its isotropic projection. (d) Spin-echo spectrum (66560 transients summed with relaxation interval of 1 s; ^{1}H decoupled) and split-t_1 STMAS spectrum (8480 transients summed for each of 48 t_1 increments of 184.5 μs; relaxation interval of 1 s; ^{1}H decoupled), together with its isotropic projection, recorded with $\nu_R = 7$ kHz on a 7-mm MAS probe. The autocorrelation STMAS diagonals in panels c and d are marked with asterisks. Chemical shifts referenced to aqueous $MgSO_4$ (via MgO MAS peak at 26 ppm).[5]

with the expected (from the XRD structure[22]) single second-order quadrupolar line shape yields $\delta_{CS} = 10$ ppm, $C_Q = 2.1$ MHz, and $\eta = 0.7$, in agreement with refs 23 and 24, although these values must be treated with caution as the experimental line shape lacks the distinctive features of the simulated line shape. The ^{25}Mg STMAS NMR spectrum of nonenriched diopside, shown in Figure 6b together with its isotropic projection, was recorded in 32 h and reveals a single Mg site with a somewhat broadened isotropic projection. Center-of-mass analysis of the ridge line shape yields $\delta_{CS} = 7$ ppm and $P_Q = C_Q(1 + \eta^2/3)^{1/2} = 2.2$ MHz in good agreement with the line shape in Figure 6a. Unlike the previous materials, this was a

natural mineralogical sample of diopside and the observed broadening may be due to structural disorder arising from partial cation substitution.

Finally, to demonstrate that ^{25}Mg STMAS NMR can distinguish inequivalent Mg sites, even at natural abundance, Figure 6c shows the ^{25}Mg spin-echo MAS spectrum (recorded in 20 h) and the STMAS spectrum (recorded in 80 h) of a 1:1 Mg at. % mixture of nonenriched brucite and diopside, while Figure 6d shows the ^{25}Mg spin-echo MAS spectrum (recorded in 18 h) and the STMAS spectrum (recorded in 113 h) of nonenriched talc ($Mg_3Si_4O_{10}(OH)_2$). The isotropic projection of the talc STMAS spectrum in Figure 6d appears to indicate two inequivalent Mg sites, possibly with the 2:1 intensity ratio expected from the XRD structure;[25] hence, we provisionally assign the two peaks to the crystallographic sites Mg2 and Mg1, respectively. Fitting of the extracted δ_2 line shape for Mg2 yields $\delta_{CS} = 16$ ppm, $C_Q = 2.1$ MHz, and $\eta = 0.3$, and these values were then used in the fitting of the spin-echo line shape to yield $\delta_{CS} = 25$ ppm, $C_Q = 2.8$ MHz, and $\eta = 1.0$ for the Mg1 site. Center-of-mass analyses of the ridge line shapes yield $\delta_{CS} = 16$ ppm and $P_Q = 2.2$ MHz for Mg2 and $\delta_{CS} = 22$ ppm and $P_Q = 3.0$ MHz for Mg1 in good agreement with the fitting results. Note, however, that we would estimate a large error in these δ_{CS} values (perhaps ± 6 ppm) since 1 ppm is only 24.5 Hz and both the second-order quadrupolar isotropic shifts and broadenings are rather large.

Conclusions

We have shown, using numerical calculations and preliminary ^{39}K and ^{25}Mg NMR experiments, that the STMAS techique holds great promise for the study of low-γ nuclei. Indeed, although two ^{25}Mg MQMAS studies that used highly ^{25}Mg-enriched materials have appeared previously,[26,27] here we have presented what we believe are the first high-resolution ^{25}Mg NMR spectra at natural abundance. Many obstacles still need to be overcome, however, if high-resolution NMR of low-γ quadrupolar nuclei is to become a method of wide utility. First, the low sensitivity (proportional to γ^3) demands the use of large-diameter MAS rotors and yet the large second-order quadrupolar broadenings (proportional to $1/\gamma$) demand the use of the highest MAS rates: currently, these requirements are mutually incompatible. A partial answer to this problem is to use very high B_0 fields, much higher than the $B_0 = 9.4$ T used here, as these would reduce the need for large-diameter rotors (sensitivity is proportional to B_0^2) as well as reducing the need for high MAS rates (second-order broadening is proportional to $1/B_0$). It should be noted, however, that the use of high B_0 fields does nothing to increase the strength of the radio frequency field ($\nu_1 = \gamma B_1/2\pi$) and STMAS is expected to retain its advantages over MQMAS for high-resolution NMR of low-γ quadrupolar nuclei. Second, the third-order quadrupolar interaction (proportional to $1/\gamma^2 B_0^2$) is likely to be a nuisance in STMAS NMR of low-γ nuclei, although again high B_0 fields will help. Third, spin-lattice (T_1) relaxation rates will be excessively slow for many low-γ nuclei. And finally, as is well-known from ^{27}Al NMR[28] and hinted at by the ^{25}Mg NMR results in Figure 6, cation disorder in many naturally occurring materials is likely to result in low-γ STMAS (and MQMAS) NMR peaks that are very broadened and will have serious consequences for sensitivity and spectral interpretation.

Acknowledgment. We are grateful to EPSRC for a studentship (N.G.D.), to the Royal Society for the award of a Leverhulme Trust Senior Research Fellowship (S.W.) and a Dorothy Hodgkin Research Fellowship (S.E.A.), to Dr R. I. Walton (Exeter) for the synthesis of enriched brucite, and to Dr Z. Gan (NHFML, Tallahassee, FL) for simulating the effects of the third-order ^{25}Mg quadrupolar interaction in brucite.

References and Notes

(1) Frydman, L.; Harwood, J. S. *J. Am. Chem. Soc.* **1995**, *117*, 5367.
(2) Massiot, D.; Touzo, B.; Trumeau, D.; Coutures, J. P.; Virlet, J.; Florian, P.; Grandinetti, P. J. *Solid State Nucl. Magn. Reson.* **1996**, *6*, 73.
(3) Amoureux, J. P.; Fernandez, C.; Steuernagel, S. *J. Magn. Reson. A* **1996**, *123*, 116.
(4) Brown, S. P.; Wimperis, S. *J. Magn. Reson.* **1997**, *128*, 42.
(5) Smith, M. E. In *Annual Reports on NMR Spectroscopy*; Webb, G. A., Ed.; Academic: New York, 2000; Vol. 43, p 121.
(6) Amoureux, J. P.; Fernandez, C.; Frydman, L. *Chem. Phys. Lett.* **1996**, *259*, 347.
(7) Amoureux, J. P.; Pruski, M.; Lang, D. P.; Fernandez, C. *J. Magn. Reson.* **1998**, *131*, 170.
(8) Gan, Z. *J. Am. Chem. Soc.* **2000**, *122*, 3242.
(9) Ashbrook, S. E.; Wimperis, S. *J. Magn. Reson.* **2002**, *156*, 269.
(10) Ashbrook, S. E.; Wimperis, S. *J. Am. Chem. Soc.* **2002**, *124*, 11602.
(11) Ashbrook, S. E.; Berry, A. J.; Hibberson, W. O.; Steuernagel S.; Wimperis, S. *J. Am. Chem. Soc.* **2003**, *125*, 11824.
(12) Ashbrook, S. E.; Wimperis, S. *Prog. NMR Spectrosc.* **2004**, *45*, 53.
(13) Wokaun, A.; Ernst, R. R. *J. Chem. Phys.* **1977**, *67*, 1752.
(14) Gerothanassis, I. P. *Prog. NMR Spectrosc.* **1987**, *19*, 267.
(15) Ojima, K.; Nishihata, Y.; Sawada, A. *Acta Crystallogr. B* **1995**, *51*, 287.
(16) Bastow, T. J. *J. Chem. Soc., Faraday Trans.* **1991**, *87*, 2453.
(17) Winkler, B.; Milman, V.; Hennion, B.; Payne, M. C.; Lee, M. H.; Lin, J. S. *Phys. Chem. Miner.* **1995**, *22*, 461.
(18) Dupree, R.; Smith, M. E. *J. Chem. Soc. Chem. Commun.* **1988**, 1483.
(19) Bastow, T. J. *Solid State Commun.* **1991**, *77*, 547.
(20) Gan, Z.; Srinivasan, P.; Quine, J. R.; Steuernagel, S.; Knott, B. *Chem. Phys. Lett.* **2003**, *367*, 163.
(21) Gan, Z. Personal communication.
(22) Redhammer, G. J. *Eur. J. Mineral.* **1998**, *10*, 439.
(23) Fiske, P. S.; Stebbins, J. F. *Am. Mineral.* **1994**, *79*, 848.
(24) Kroeker, S.; Stebbins, J. F. *Am. Mineral.* **2000**, *85*, 1459.
(25) Perdikatsis, B.; Burzlaff, H. *Z. Kristallogr.* **1981**, *156*, 177.
(26) Sham, S.; Wu, G. *Inorg. Chem.* **2000**, *39*, 4.
(27) Grant, C. V.; Frydman, V.; Frydman, L. *J. Am. Chem. Soc.* **2000**, *122*, 11743.
(28) McManus, J.; Ashbrook, S. E.; MacKenzie, K. J. D.; Wimperis, S. *J. Non-Cryst. Solids* **2001**, *282*, 278.